Atmos. Chem. Phys. Discuss., https://doi.org/10.5194/acp-2018-279
Manuscript under review for journal Atmos. Chem. Phys.
Discussion started: 1 June 2018

Atmospheric Chemistry and Physics
Discussions

Relationships between the planetary boundary layer height and surface pollutants derived from lidar observations over China

Tianning Su[1], Zhanqing Li[1,2*], Ralph Kahn[3]

[1]Department of Atmospheric and Oceanic Sciences & ESSIC, University of Maryland, College Park, Maryland 20740, USA

[2]State Key Laboratory of Earth Surface Processes and Resource Ecology and College of Global Change and Earth System Science, Beijing Normal University, 100875, Beijing, China

[3]Climate and Radiation Laboratory, Earth Science Division, NASA Goddard Space Flight Center, Greenbelt, MD, USA

∗ *Correspondence to:* Zhanqing Li (zli@atmos.umd.edu)

Abstract. The frequent occurrence of severe air pollution episodes in China has raised great concerns with the public and scientific communities. Planetary boundary layer height (PBLH) is a key factor in the vertical mixing and dilution of near-surface pollutants. However, the relationship between PBLH and surface pollutants, especially particulate matter (PM) concentration, across the whole of China, is not yet well understood. We investigate this issue at ~1500 surface stations using PBLH derived from space-borne and ground-based lidar, and discuss the influence of topography and meteorological variables on the PBLH-PM relationship. A generally negative correlation is observed between PM and the PBLH, albeit varying greatly in magnitude with location and season. Correlations are much weaker over the highlands than plains regions, which may be associated with lower pollution levels and mountain breezes. The influence of horizontal transport on surface PM is considered as well, manifested as a negative correlation between surface PM and wind speed over the whole nation. Strong wind with clean upwind sources plays a dominant role in removing pollutants, and leads to weak PBLH-PM correlation. A ventilation rate is introduced to jointly consider horizontal and vertical dispersion, which has the largest impact on surface pollutant accumulation over the North China Plain. Aerosol absorption feedbacks also appear to affect the PBLH-PM relationship, as revealed via comparing air pollution in Beijing and Hong Kong. Absorbing aerosols in high concentrations likely contribute to the significant PBLH-PM correlation over the North China Plain (e.g., during winter). As major precursor emissions for secondary aerosols, sulfur dioxide, nitrogen dioxide, and carbon monoxide have similar negative responses to increased PBLH, whereas ozone is positively correlated with PBLH over most regions, which may be caused by heterogeneous reactions and photolysis rates.

1. Introduction

In the past few decades, China has been suffering from severe air pollution, caused by both particulate matter (PM) and anthropogenic gases. PM pollutants are of greatest concern to the public partly because they are much more visible (Chan and Yao, 2008; J. Li et al., 2016), and because they have discernible adverse effects on human health. Moreover, airborne particles critically impact Earth's climate through aerosol direct and indirect effects (Ackerman et al., 2004; Boucher et al., 2013; Guo et al., 2017; Kiehl et al., 1993; Li et al., 2016; 2017a).

Multiple factors contribute to the severe air pollution over China. Strong emission due to rapid urbanization and industrialization is a primary cause. Meanwhile, meteorological conditions and diffusion within the planetary boundary layer (PBL) also play important roles in the exchange between polluted and clean air. Among the meteorological parameters of importance, the PBL height (PBLH) can be related to the vertical mixing, affecting the dilution of pollutants emitted near the ground through various interactions and feedback mechanisms (Emeis and Schäfer. 2006; Seibert et al., 2010; Su et al., 2017a). Therefore, PBLH is a critical parameter affecting near-surface air quality, and it serves as a key input for chemistry transport models (Knote et al., 2015; LeMone et al., 2013). The PBLH can significantly impact aerosol vertical structure, as the bulk of locally generated pollutants tends to be concentrated within this layer. Turbulent mixing within the PBL can account for much of the variability in near-surface air quality. On the other hand, aerosols can have important feedbacks on PBLH, depending on the aerosol properties, especially their light absorption (e.g., black, organic, and brown carbon; Wang et al., 2013). Multiple studies demonstrate that absorbing aerosols tend to affect surface pollution in China through their interactions with PBL meteorology (Ding et al., 2016; Miao et al., 2016; Dong et al., 2017; Petäjä et al., 2016). However, the importance and magnitude of aerosol feedback to

PBLH are still uncertain, as the feedback is closely related to aerosol structure, and may be weakened by strong turbulence in PBL. Li et al. (2017b) give evidence of this in a review of the interaction between the PBL and air pollution.

There are various methods for identifying the PBLH. The traditional and most common ones are gradient (e.g., Johnson et al., 2001; Liu and Liang, 2010) and Richardson number methods (e.g., Vogelezang and Holtslag, 1996), both of which are typically based on temperature, pressure, humidity, and wind speed profiles obtained by radiosondes. By using fine-resolution radiosonde observations, Guo et al. (2016) obtained the first comprehensive PBLH climatology over China. Ground-based lidars, such as the micropulse lidar (MPL), are also widely used to derive the PBLH (e.g., Hägeli et al., 2000; He et al., 2008; Sawyer and Li, 2013; Tucker et al., 2009; Yang et al., 2013). The lidar-based PBLH identification relies on the principle that a temperature inversion often exists at the top of the PBL, trapping moisture and aerosols (Seibert et al., 2000), which causes a sharp decrease in the aerosol backscatter signal at the PBL upper boundary. However, using ground-based observations to retrieve the PBLH suffers from poor spatial coverage and very limited sampling. The Cloud-Aerosol Lidar with Orthogonal Polarization (CALIOP) on board the Cloud-Aerosol Lidar and Infrared Pathfinder Satellite Observations (CALIPSO) satellite (Winker et al., 2007), an operational spaceborne lidar, can retrieve cloud and aerosol vertical distributions at moderate vertical resolution, complementing ground-based PBLH measurements. Several studies already demonstrate both the effectiveness and the limitations of using CALIPSO data for PBLH detection, showing sound but highly variable agreement with those from radiosonde- and MPL-based PBLH results (Su et al., 2017b; Leventidou et al., 2013; Liu et al., 2015; Zhang et al., 2016).

Several studies have explored the relationship between PBLH and surface pollutants in China. Tang et al. (2016) used ceilometer measurements to derive long-term PBLH behavior in Beijing, further demonstrating the strong correlation between the PBLH and surface visibility under high humidity conditions. Wang et al. (2017) classified atmospheric diffusion conditions based on PBLH and wind speed, and identified significant surface PM changes that also varied with dispersion conditions. Miao et al. (2017) investigated the relationship between summertime PBLH and surface PM, and discussed the impact of synoptic patterns on the development and structure of the PBL. Qu et al. (2017) derived one-year PBLH variations from lidar in Nanjing, and presented the strong correlation between PBLH and $PM_{2.5}$, especially for hazy and foggy days.

However, the majority of the studies mostly employ data only at a few stations. Yet, the interaction between PBLH and surface pollutants under different topographic and meteorological conditions is not well understood. Assessing the relationship between PM and the PBLH quantitatively over the entire country, is of particular significance. PBL turbulence is not the only factor affecting air quality, so there can be large regional differences in the interaction between the PBLH and PM. As such, the contributions of various factors to the PBLH-PM relationship may be disclosed, that thus warrant a further investigation.

Given the above-mentioned limitations, this study presents a comprehensive exploration of the relationship between the PBLH and surface pollutants over China, for a wide range of atmospheric, aerosol and topographic conditions. Since 2012, China has drastically increased the number of instruments and implemented rigorous quality control measures to measure hourly pollutant concentrations nationally, of much better quality than previously available. The pollutant data derived from surface observations, along with CALIPSO measurements, offer us an opportunity to investigate the impact of PBLH on air quality on a nationwide basis. Regional characteristics and seasonal variations are considered. Moreover, multiple factors related to the interaction between the PBLH and PM are investigated, including surface topography, horizontal transport, and aerosol type. The relationships between the PBLH and several gas pollutants are also presented. These empirical relationships between PBLH and surface pollutants are aimed at improving our understanding and forecasting ability for air pollution, as well as helping refine meteorological and atmospheric chemistry models.

2. Data and Method

2.1. Surface observation sites

The topography of China is presented in Figure 1a, and the pink rectangles outline the four regions of interest (ROI) for the current study: northeast China (NEC), the Yangtze River Delta (YRD), Pearl River Delta (PRD), and North China Plain (NCP). The environmental monitoring station locations are indicated with red dots in Figure 1b. They routinely measure hourly pollutant data, including PM with diameters ≤ 2.5 and 10 μm ($PM_{2.5}$ and PM_{10}, respectively), sulfur dioxide (SO_2), nitrogen dioxide (NO_2), carbon monoxide (CO), and ozone (O_3). The locations of meteorological stations operated by the China Meteorological Administration are indicated in Figure 1c. We use wind speed and wind direction data obtained at these stations. As shown in Figure 1d, blue lines represent the ground tracks over China for the daytime overpasses of CALIPSO. To match the CALIPSO retrievals with surface pollutant and meteorological data, we average the available CALIPSO retrievals within 35 km of the surface stations, and use the noontime surface data, where "noontime" refers to results averaged from 1300 to 1500 China standard time (CST). We also utilized the MPL data at Beijing and sun-photometer data at Beijing and Hong Kong, two megacities located over NCP and PRD respectively. The MPL located at Beijing was operated continuously by Peking University (39.99°N, 116.31°E) from Apr 2016 to Dec 2017, with a temporal resolution of 15s and a vertical resolution of 15m. The near-surface blind zones for both lidars

Atmos. Chem. Phys. Discuss., https://doi.org/10.5194/acp-2018-279
Manuscript under review for journal Atmos. Chem. Phys.
Discussion started: 1 June 2018

Atmospheric Chemistry and Physics Discussions

are around 150 meters. Background subtraction, saturation, after-pulse, overlap, and range corrections are applied to raw MPL data (He et al., 2008, Yang et al., 2013). In this study, Level 1.5 AOD at 550/440 nm and single-scattering albedo (SSA) at 675 nm at Beijing RADI (40°N, 116.38°E) and Hong Kong PolyU (22.3°N, 114.18°E) Aerosol Robotic Network (AERONET) sites with hourly time resolution are used.

2.2. PBLH derived from MPL

MPL data from Beijing were used to retrieve the PBLH for this study. Multiple methods have been developed for retrieving the PBLH from MPL measurements, such as signal threshold (Melfi et al., 1985), maximum of the signal variance (Hooper and Eloranta, 1986), minimum of the signal profile derivative (Flamant et al., 1997), and wavelet transform (Cohn and Angevine, 2000; Davis et al., 2000). In this study, we implement a well-established method by Yang et al. (2013) to derive the PBLH from MPL data, with a few modifications. This method can handle all possible weather conditions and aerosol layer structures, and is tested to be suitable for processing long-term lidar data. Initially, the first derivative of a Gaussian filter with a wavelet dilation of 60 m is applied to smooth the vertical profile of MPL signals, and to produce the gradient profile. The aerosol stratification structure is indicated by multiple valleys and peaks in the gradient profile. To exclude misidentified elevated aerosol layers above the PBL, the first significant peak in the gradient profile (if one exists) is considered the upper limit in searching for the PBL top. Then, the height of the deepest valley in the gradient profile is attributed to the PBLH; discontinuous or false results caused by clouds are subsequently eliminated manually. In this study, we further estimated the shot noise (σ) induced by background light and dark current for each profile, and then added threshold values of $\pm 3\sigma$ to the identified peaks and valleys of this profile to reduce the

Atmos. Chem. Phys. Discuss., https://doi.org/10.5194/acp-2018-279
Manuscript under review for journal Atmos. Chem. Phys.
Discussion started: 1 June 2018

Atmospheric Chemistry and Physics Discussions
Open Access

impact of noise. To validate MPL-derived PBLH, the values are compared with summertime radiosonde PBLH data at 14:00 CST retrieved at Beijing station (39.80°N, 116.47°E) from potential temperature profiles by the Richardson number methods (e.g., Vogelezang and Holtslag, 1996). Figure S1a shows good agreement (R=0.7) between MPL- and radiosonde-derived PBLHs over Beijing.

2.3. PBLH derived from CALIPSO

CALIOP aboard the CALIPSO platform is the first space-borne lidar optimized for aerosol and cloud profiling. As part of the Afternoon satellite constellation, or A-Train (L'Ecuyer and Jiang, 2010), CALIPSO is in a 705-km Sun-synchronous polar orbit between 82°N and 82°S, with equator crossings at approximately 1330 and 0130 local time and a 16-day repeat cycle (Winker et al., 2007, 2009). CALIOP measures the total attenuated backscatter-coefficient (TAB) with a horizontal resolution of 1/3 km and a vertical resolution of 30 m in the low and middle troposphere, and has two channels (532 and 1064 nm). As the nighttime heavy surface inversion and residual layers tend to complicate the identification of the PBLH, we only utilize daytime TAB data (Level 1B) in this study. For retrieving the PBLH from CALIPSO, we typically use the maximum standard deviation (MSD) method, which was first developed by Jordan et al. (2010) and then modified by Su et al. (2017b). In general, it determines the PBLH as the lowest occurrence of a local maximum in the standard deviation of the backscatter profile, collocated with a maximum in the backscatter itself. The PBLH retrieval range (0.3~4km), surface noise check, and removal of attenuating and overlying clouds are subsequently included in this method. In addition, due to the viewing geometry of the instrument, we define a constraint function:

$$\beta(i) = \max\{f(i+2), f(i+1)\} - \min\{f(i), f(i-1)\} \quad , \qquad (1)$$

where $f(\mathrm{i}+2)$, $f(\mathrm{i}+1)$, $f(\mathrm{i})$, $f(\mathrm{i}-1)$ are four adjacent altitude bins in the 532-nm TAB and where the altitude decreases with increasing bin number i. To eliminate the local standard deviation maximum caused by signal attenuation, we add the constraint $\beta > 0$, and locate the PBLH at the top of the aerosol layer. Moreover, we also use the wavelet covariance transform (WCT) method to retrieve the PBLH, and this retrieval serves as a constraint. We eliminate cases when the difference between the MSD and WCT retrievals is above 0.5 km, to increase the reliability of the MSD retrievals.

Due to the high signal-to-noise ratio and reliability of MPL measurements, we use MPL-derived PBLH to test the CALIPSO retrievals. The comparison between CALIPSO- and MPL-derived PBLH at Beijing and Hong Kong (result from Su et al., 2017b) are shown in Figure S1b-c. Reasonable agreement between CALIPSO- and MPL-derived PBLHs at these two sites is shown. The correlation coefficients are above 0.6, which is similar to results from previous studies (e.g., Liu et al., 2015; Su et al., 2017b; Zhang et al., 2016). Besides the differences in signal-to-noise ratio, the 10-40 km distance between the MPL station and CALIPSO orbit also contributes to the differences between MPL- and CALIPSO-derived PBLH.

2.4. MODIS AOD data

The MODIS instruments on board Terra and Aqua have 2330-km swath widths, and provide daily AOD data with near-global coverage. In this study, we use Collection 6 MODIS level-2 AOD products from the Aqua satellite at 550 nm (available at: https://www.nasa.gov/langley). AOD data are archived with a nominal spatial resolution of 10 km × 10 km, and the data are averaged within 30 km radius around the environmental stations to match with surface PM data. The MODIS land AOD accuracy is reported to be $\pm$(0.05+15% AERONET AOD) (Levy et al., 2010).

Atmos. Chem. Phys. Discuss., https://doi.org/10.5194/acp-2018-279
Manuscript under review for journal Atmos. Chem. Phys.
Discussion started: 1 June 2018

3. Results

3.1. Climatological patterns of PBLH and surface pollutants

The climatology of the PBLH, especially its seasonal variability, is very important for air-pollution-related studies. We utilized the CALIPSO measurements during the period 2006 through 2017 to represent the spatial distribution of seasonal mean PBLH, as shown in Figure 2a-d. A smoothing window of 20 km was applied to the original PBLH data at 1/3 km horizontal resolution. For comparison, we also used the PBLH data obtained from the Modern Era-Retrospective Reanalysis for Research and Applications (MERRA) reanalysis dataset with a spatial resolution of 2/3°×1/2° (longitude-latitude). The MERRA reanalysis data uses a new version of the Goddard Earth Observing System Data Assimilation System Version 5 (GEOS-5). The seasonal climatological patterns of MERRA-derived PBLH are presented in Figure 2e-h for the same period. In general, the climatological pattern of MERRA PBLH is similar to that of CALIPSO, though the MERRA values are higher in spring and summer, and the peak values are lower in autumn and winter. Both CALIPSO and MERRA PBLHs are generally shallower in winter, when the development of the PBL is typically suppressed by the weaker solar radiation reaching the surface, and is generally higher in summer, especially for inland regions.

Note that there are still large differences between CALIPSO- and MERRA-derived PBLH climatological patterns, which can be attributed to sampling biases, different definitions, and model uncertainty. First, since the spatial coverage and time resolution are quite different between the CALIPSO and MERRA datasets, the sampling used to calculate the climatologies are quite different. Moreover, MERRA PBLHs are derived from turbulent fluxes computed by the model, whereas CALIPSO usually identifies the top height of an aerosol-rich layer. Although turbulent fluxes would significantly affect aerosol structures, the different definitions still can cause large differences between CALIPSO and MERRA PBLHs. The detailed relationship between of CALIPSO- and MERRA PBLHs is presented in Figure S1d. CALIPSO PBLH exhibits considerable differences from MERRA results, with a correlation coefficients of ~0.4, indicating that the observations presented here will likely be useful for future model refinement.

The seasonal mean values of CALIPSO and MERRA PBLHs over four ROIs are presented in Table 1. Broadly speaking, the differences between CALIPSO and MERRA PBLHs are much smaller than their standard deviations. PBLH shows strong seasonality over NCP and NEC, ranging from ~0.9 km (winter) to 1.5 km (summer). As the seasonal variation of PBLH is much smaller than the standard deviation over PRD and YRD, the seasonal patterns are not clear for these two regions. MERRA PBLH shows similar seasonal means with CALIPSO over NCP, with differences of ~0.1km, and shows the largest differences (0.5km) with CALIPSO PBLH over NEC during winter.

Correspondingly, the seasonal means and standard deviations over four ROIs are listed in Table 1. The $PM_{2.5}$ seasonal pattern is generally opposite that of PBLH, with the lowest values in summer and the highest in winter. Since a high PBLH facilitates the vertical dilution and dissipation of air pollution, the contrasting patterns of PBLH and $PM_{2.5}$ are consistent with expectation, although one cannot assure their causal relationship from these plots alone. As this is a major polluted region, both PBLH and $PM_{2.5}$ show particularly strong seasonality over NCP. PRD is a relatively clean region, and $PM_{2.5}$ maintains low values (<50 μg m^{-3}) through all seasons. The spatial distributions of PM_{10}, and multiple gas pollutants (SO_2/NO_2/CO/O_3) climatologies are shown in Figure S2. The seasonal and regional patterns of $PM_{2.5}$, PM_{10}, SO_2, NO_2, and CO all show their highest values in winter and lowest in summer, similar to $PM_{2.5}$. However, unlike the other pollutants, O_3 reaches its highest values during summer. These patterns are discussed in more detail in subsequent sections.

3.2. Regional relationships between PM and PBLH

If the common factor driving large-scale variations in both PM and PBLH is meteorology, a regional analysis of their relationship could elucidate the meteorological impacts. We investigate the CALIPSO-PBLH and surface $PM_{2.5}$ data case by case. The scatterplots for annually aggregated PBLH versus surface $PM_{2.5}$ for the four ROI are shown in Figure 3. Although there is a large spread and regional differences, the negative correlations between PBLH and $PM_{2.5}$ are seen in all ROIs. PBLH values show the most negative correlation with $PM_{2.5}$ over the NCP, with a correlation coefficient of -0.36. PBLH also shows significant negative correlation with $PM_{2.5}$ over YRD and NEC, with correlation coefficients of -0.24 and -0.15, respectively. (Hereafter, "significant" indicates the correlation is statistically significant at the 95% confidence level.) The weak PBLH correlation with $PM_{2.5}$ over the PRD is not statistically significant. The relationships between PBLH and PM_{10} are similar to those with $PM_{2.5}$, except with larger spreads, because the magnitudes of PM_{10} are larger than those of $PM_{2.5}$ (Figure S3). Compared to CALIPSO data, the MPL has a much higher signal-to-noise ratio and can continuously observe at one location. Therefore, we compare the relationships between MPL-derived PBLH and $PM_{2.5}$ with those from CALIPSO at Beijing (Figure S4). Similar to the relationship derived from CALIPSO, the PBLH shows a significantly nonlinear relationship with $PM_{2.5}$ over Beijing (a major city in the NCP).

We notice that the ranges of $PM_{2.5}$ for these ROIs are significantly different; therefore, the background pollution level is likely to be an important factor for the PBLH-PM relationship. We also normalize the $PM_{2.5}$ by MODIS AOD, a widely used parameter to represent the columnar aerosol amount, to qualitatively account for background or transported aerosol that is not concentrated in the PBL. The

Atmos. Chem. Phys. Discuss., https://doi.org/10.5194/acp-2018-279
Manuscript under review for journal Atmos. Chem. Phys.
Discussion started: 1 June 2018

relationship between PBLH and $PM_{2.5}$/AOD over four ROIs are presented in Figure 4. Clearly, after normalizing $PM_{2.5}$ by AOD, the spread of these scatter plots and the regional differences are significantly reduced, and the correlations became more significant for all ROIs, especially for PRD. This is because transported aerosol aloft can contribute to variability in total column AOD that is unrelated to the PBLH.

Figure S5 provides a closer look at the regional differences among individual sites. As with Figure 3, the most negative correlations between PBLH and $PM_{2.5}$ appear over the NCP, likely a testament to intense PBL-aerosol interactions, which may be caused by concentrated local sources. Several scattered sites show positive correlations between PBLH and $PM_{2.5}$, though they are generally not significant. Note that the PBLH-$PM_{2.5}$ correlations are apparently stronger for heavily polluted regions, than for clean regions. However, after normalizing $PM_{2.5}$ by AOD, the correlations are improved preferentially for clean regions (where aerosol aloft makes a larger fractional contribution to the AOD), and thus, the differences between clean and polluted regions are reduced (Figure S6). It further indicates that the background pollution level plays a critical role in the PBLH-PM relationship.

As the NCP experiences the most pronounced seasonality in both PBLH and $PM_{2.5}$, their relationship over this region also shows the most prominent seasonal differences (Figure S5c-f). Figure 5 focuses on the seasonal dependence of the PBLH and $PM_{2.5}$ relationship over the NCP. The mean slope for this region is ~90 $\mu g\ m^{-3}\ km^{-1}$ during winter, and is only ~20 $\mu g\ m^{-3}\ km^{-1}$ in summer. For comparison, the annual aggregated relationship between PBLH and $PM_{2.5}$ is presented in Figure 5e. $PM_{2.5}$ concentrations do not increase linearly with decreasing PBLH. Specifically, $PM_{2.5}$ increases rapidly with decreasing PBLH when PBLH is lower than 1 km, but changes much more slowly for PBLH > 1.5 km. The seasonal mean values for $PM_{2.5}$ and PBLH are presented as colored dots in Figure 5e, and the whiskers represent the standard deviations. For winter, the PBLH is generally shallow, $PM_{2.5}$

concentrations are high, and thus PBLH shows the most significant negative correlation with $PM_{2.5}$. Conversely, in summer, the PBLH is generally higher, $PM_{2.5}$ concentrations are lower, and the PBLH-$PM_{2.5}$ relationship is virtually flat. Such seasonally distinct PBLH-$PM_{2.5}$ relationships have not previously been studied quantitatively, and can contribute to improving $PM_{2.5}$ predictions.

3.3. Association with horizontal transport

The PBLH mainly affects the vertical mixing and dispersion of air pollution, but horizontal transport also plays a critical role in surface air quality. Figure 6a-b present the PBLH-$PM_{2.5}$ relationships over China under strong wind (WS>4m s^{-1}) and weak wind (WS<4m s^{-1}) conditions. In addition, Figure 6c-d show the aerosol extinction profiles as a function of PBLH under strong and weak wind conditions. The aerosols extinction coefficients are retrieved by the MPLs at Beijing, and the Klett method is applied (Klett, 1985). Under strong wind conditions, $PM_{2.5}$ is much less sensitive to PBLH than for weak wind. In both strong and weak wind conditions, aerosol structure changes systematically with PBLH, and sharp aerosol extinction gradients appear at the top of the PBL. Nonetheless, under strong wind, the aerosol extinction is typically low in the PBL, and the surface extinction is even lower than the extinction at PBL top. In this situation, the strong wind likely plays a dominant role in affecting $PM_{2.5}$ concentration. Under weak wind, the response of near-surface pollutants to PBLH is highly nonlinear, and both aerosol extinction and $PM_{2.5}$ fall rapidly as the PBLH increases from 600m to 1200m.

We further consider the relationship between PBLH-$PM_{2.5}$ under different wind-direction regimes for Beijing. Two different regimes are easy to identify: a northerly wind and a southerly wind; these are divided by the red line in Figure 7a. The northerly air comes from arid and semiarid regions in northwest China and Mongolia, and is usually strong and clean. The southerly wind comes from the southern part of the NCP, with high humidity and aerosol content. To relate the connections between WS, PBLH, and surface air quality, at least qualitatively, we define the ventilation rate (VR) as VR = WS × PBLH (Tie et al., 2015). Figures 7b-e present the PBLH-$PM_{2.5}$ and VR-$PM_{2.5}$ relationships under southerly wind and northerly wind conditions, respectively. For all wind conditions, VR shows reciprocal relationship with surface $PM_{2.5}$. Under northerly wind conditions, both PBLH-$PM_{2.5}$ and VR-$PM_{2.5}$ relationships are flatter and have lower correlation coefficients. The northerly wind is apparently effective in removing pollutants and may play a dominant role in affecting air quality. For the southerly wind, the $PM_{2.5}$ concentration is highly sensitive to PBLH and VR values.

To further illustrate the coupling effects of PBLH and WS on surface pollutants, Figure 8a presents the relationship between noontime WS and $PM_{2.5}$ concentration across China. Overall, WS is negatively correlated with $PM_{2.5}$, although a few stations over southwest China show positive correlations. A negative correlation might be expected in general, as strong winds can be effective at removing air pollutants; however, other factors such as wind direction must also be considered, as, for example, upwind sources could increase pollution under higher wind conditions. There are positive correlations between PBLH and near-surface WS in most cases (Figure S7a), and thus, low PBLH and weak WS tend to occur together over much of China. These unfavorable meteorological conditions for air quality would exacerbate severe pollution episodes.

To consider horizontal and vertical dispersion jointly, we investigate the nationwide relationships between VR and $PM_{2.5}$. In general, VR is overwhelmingly negative correlated with surface $PM_{2.5}$ (Figure S7b). Based on Figure 8a, VR is typically reciprocal to $PM_{2.5}$ for all wind conditions, and thus, we use the function $f(x) = {}^{A}/_{x}$ to characterize the relationship between VR and $PM_{2.5}$, with A as the fitting parameter, and x is VR, and $f(x)$ is $PM_{2.5}$. The spatial distribution of A, presented in Figure 8b, shows the largest values over the NCP, indicating that the $PM_{2.5}$ concentration is highly sensitive to the VR there. Moreover, VRs are relatively large over the coastal areas, where sea-land breezes could play a role in dispersing air pollution. The detailed relationships and fitting functions for four ROIs are presented in Figure S8. We note that although there are large regional differences in the PBLH-$PM_{2.5}$ relationship (Figure 3), the VR-$PM_{2.5}$ relationships are similar for the different study regions. Therefore, by combining vertical and horizontal dispersion conditions, the overall VR apparently has a similar effect on $PM_{2.5}$ for all four ROI.

3.4. Correlations with topography

The PBL structure and $PM_{2.5}$ concentration can both be affected by topography. We also divided all the sites into two categories based on elevation: plains (elevation < 0.5 km) and highland (elevation > 1 km). Figure 9a-d presents the correlation coefficients and slopes between $PM_{2.5}$ and PBLH for the plains and highland areas. Much stronger correlations exist in the plains than the highlands. A reciprocal correlation is shown between station elevation and the PBLH-$PM_{2.5}$ slope (Figure 9e). The magnitudes of slopes decrease dramatically with elevation increase between 0 and 500 m. Local emissions also affect aerosol loading, and differences between plains and highland areas regarding local source activity could be important here as well. Figure 9e shows that the low-elevation regions are typically more polluted than highland areas, and the magnitudes of PBLH-$PM_{2.5}$ slopes also tend to be higher.

Returning to Figure S5, much stronger correlations for PBLH-$PM_{2.5}$ relationships are found over polluted regions, which also correspond to the plains areas due to strong local emissions. Therefore, high aerosol loading is likely to be another factor contributing to the strong correlation between PBLH and $PM_{2.5}$ over the plains, whereas the low $PM_{2.5}$ concentration may contribute to the weak PBLH- $PM_{2.5}$

correlation over the highlands.

In addition, horizontal transport is associated with topography. Thus, we illustrate the distribution of WS for plains and highland areas in Figure 9f. Clearly, WS is generally larger for highland areas, especially for strong wind cases. In fact, the 10% and 25% quantiles of WS are nearly the same between plains and highland areas, whereas there are apparent differences in the 75% and 90% quantiles. Strong wind cases account for 37% of the total over highland areas, and only account for 27% of the total over the plains. As discussed in section 3.3, strong wind can effectively remove surface pollutants, and can play a dominant role in affecting pollution levels. In this situation, PBLH might not play as critical a role in PM concentration. Thus, mountain slope winds, along with less local emission, are likely to be leading factors accounting for the differences in PBLH-$PM_{2.5}$ correlations between plains and highland areas.

3.5. Correlations between gaseous pollutants and PBLH

Secondary aerosol contributes significantly to the surface PM concentration over China (Huang et al., 2014). Multiple gas pollutants, such as SO_2, NO_2, and CO, are major precursor emissions for the formation of secondary aerosols, which are closely related to $PM_{2.5}$ concentration (Guo et al., 2014; Wang et al., 2016). Further, the near-surface concentrations of these gaseous pollutants can also have severely negative effects on the environment and human health. We investigate the relationships between gaseous pollutants and the PBLH due to their importance, by matching the CALIPSO PBLH with SO_2/NO_2/CO/O_3 concentrations obtained from surface stations (Figure 10). Again, the relationships between CALIPSO PBLH and SO_2/NO_2/CO/O_3 are similar to those derived from MPLs (Figure S4). For SO_2, NO_2, and CO, the correlations with PBLH are similar to the PBLH-PM correlations over NCP, but slightly weaker.

Similar to PBLH-PM relationships, the correlations between PBLH and SO_2/NO_2/CO are negative for all ROIs. This is understandable, because the PBLH is likely to play a role in the vertical dilution and dissipation of most gaseous pollutants. However, O_3 shows a positive correlation with PBLH for all ROIs, which might be due to O_3 photochemistry. As radiation reaching the surface increases, convection is enhanced and the PBLH tends to grow higher. At the same time, increased insolation with sufficient precursor emissions (NO_x, CO, and VOC_s) can increase the net photochemical production of O_3. Therefore, higher O_3 concentrations and high PBLH could occur together. Moreover, when the PBL is shallow and aerosol concentration is high, heterogeneous reactions on surfaces of multiple aerosols (e.g. sulfate, mineral dust, and organic carbon aerosols) can uptake ozone precursors such as NO_x and N_2O_5, and thus, reduce the ozone production (Ravishankara, 1997; Jacob., 2000). And Liao and Seinfeld (2005) found that the high aerosol loading reduces ozone concentrations by 25-30% through heterogeneous reactions over eastern China. Taken together, decreased PBLH correlates with increased near-surface aerosol concentration, leading to a reduction in precursors required for O_3 production, and an increase in O_3 destruction by heterogeneous reactions. This could explain, at least qualitatively, the positive PBLH-O_3 relationship.

3.6. Potential feedback of absorbing aerosols

Depending on their radiative properties, aerosols can have feedbacks on the PBLH. Multiple studies point out a positive feedback between absorbing aerosols and the PBLH (Ding et al., 2016; Miao et al., 2016; Petäjä et al., 2016). Using lidars and AERONET data, we examine the link between the PBLH-$PM_{2.5}$ relationship and particle optical properties over Beijing and Hong Kong. We utilized AERONET SSA data to classify aerosols as absorbing (SSA $\leq$ 0.85) or weakly absorbing (SSA $>$ 0.9). The correlation between PBLH and $PM_{2.5}$ is much stronger for absorbing cases over both Beijing and Hong Kong (Figure 11). Noted the PBLHs over Beijing are obtained from MPL. Due to lack of available MPL data, the PBLHs over Hong Kong are calculated by CALIPSO. Since AERONET SSA is more reliable for the cases when AOD at 440nm is above 0.4 (Schafer et al., 2014), Figure S9 shows the PBLH-$PM_{2.5}$ relationship for absorbing and weakly absorbing cases over Beijing with a constraint of $AOD_{440}>0.4$. The PBLH-$PM_{2.5}$ correlation remains considerably stronger for absorbing than weakly absorbing cases. Under sufficient aerosol loading, we found PBLH-$PM_{2.5}$ correlations become stronger for both absorbing and weakly absorbing cases. In addition, there are many more strongly absorbing cases for Beijing (~35%) than for Hong Kong (~10%), and the total PBLH-$PM_{2.5}$ correlation is much stronger over Beijing.

Moreover, we show how absorbing optical depths over Beijing and Hong Kong correlate with the general PBLH-$PM_{2.5}$ relationship in Figure 11e-f. Under highly absorbing optical depth conditions, $PM_{2.5}$ tends to be higher for a given PBLH. Large absorbing optical depths in Beijing offer great potential for reducing the radiation reaching the surface, likely reducing the PBLH, and at the same time, heating the middle and upper PBL, which would tend to cause a temperature inversion and increase the stability in the PBL. The strongly absorbing aerosols with high loading are likely to give important feedback to PBLH, and may contribute to the strong correlation between the PBLH and PM over Beijing. Other factors could be involved, such as the vertical distribution of aerosol, the insolation, and the actual SSA of the particles; further examination of these phenomena is beyond the scope of the current paper.

4. Discussion and conclusions

Based on ten years of CALIPSO measurements and other environmental data obtained from more than 1500 stations, large-scale relationships between PBLH and PM are assessed over China. We observe widespread negative correlations, albeit varying greatly in magnitude and seasonal timing by region. Nonlinear responses of $PM_{2.5}$ to PBLH evolution are found, especially for NCP, the most polluted region of China. Strongest PBLH-$PM_{2.5}$ interaction is found when the PBLH is shallow and $PM_{2.5}$ concentration is high, which typically corresponds to the wintertime cases. Specifically, the negative correlation between PBLH and $PM_{2.5}$ is most significant during winter. Moreover, we find that regional differences in the PBLH-PM relationships are correlated with topography. Strong correlations between PBLHs and aerosols occur in low-altitude regions. This might be related to the more frequent air stagnation and strong local emission over China's plains, as well as a greater concentration of emission sources. The mountain breezes and a larger fraction of transported aerosol above the PBL help weaken the PBLH-PM correlation over highland areas.

As pollution levels can affect the PBLH-$PM_{2.5}$ relationship, we normalized $PM_{2.5}$ by MODIS total-column AOD to account for the background aerosol in different regions. Comparing to PBLH-$PM_{2.5}$ correlations, the correlations between PBLH and normalized $PM_{2.5}$ ($PM_{2.5}$/AOD) increased significantly for clean regions, resulting in smaller regional differences overall. Retrieving surface $PM_{2.5}$ from AOD constraints has been investigated in many studies. The detailed relationships between PBLH and $PM_{2.5}$/AOD over different ROIs are also expected to be significant for relating $PM_{2.5}$ to remotely sensed AOD, due to the way PBLH affects near-surface aerosol concentration.

Horizontal transport also shows significant inverse correlation with $PM_{2.5}$ concentrations. WS and PBLH tend to be positively correlated with each other in the study regions, which means meteorologically favorable horizontal and vertical dispersion conditions are likely to occur together. Wind direction can also significantly affect the PBLH-PM relationship. Strong wind with clean upwind sources plays a dominant role in improving air quality, and leads to weak PBLH-PM correlation. The combination of

WS and PBLH, representing a "ventilation rate," shows a reciprocal correlation with surface PM in all the regions studied. VR also is found to have the largest impact on surface pollutant accumulation over the NCP.

As major precursor emissions for secondary aerosols, SO_2, NO_2, and CO show negative correlations with PBLH, similar to the PBLH-PM correlations. However, O_3 is positively correlated with PBLH over most regions, which may be caused by heterogeneous reactions and photolysis rates. This observation merits further investigation using comprehensive measurements of chemical properties together with necessary simulations from atmospheric chemistry model to ascertain the causes of the positive PBLH-O_3 correlations.

As revealed by observations at Beijing and Hong Kong, absorbing aerosols with sufficient aerosol loading likely contribute the strong PBLH-PM correlation. Large absorbing AOD would reduce the radiation reaching the surface and heat the middle and upper PBL, which could increase the stability in the PBL, representing a direct interaction between PBLH and PM. Much more strongly absorbing cases for NCP than for PRD appear to contribute to the large contrast for PBLH-PM correlations between these two regions. On the other hand, despite the strong correlations for absorbing cases with sufficient aerosol loading, identifying a causal relationship between them is still elusive, as confounding factors, such as aerosol vertical distribution, aerosol microphysical properties, ambient insolation, and meteorological conditions, could all be involved. This merits further analysis using more comprehensive measurements from field experiments, from which integrated aerosol conditions and model simulations can account for aerosol radiative forcing while controlling all the other relevant variables

Our work comprehensively covers the relationships between PBLH and surface pollutants over larger spatial scales in China. Multiple factors, such as horizontal transport, topography, and aerosol optical properties, are found to be highly correlated with PBLH and near-surface aerosol concentration. Such information can help improve our understanding for the complex interactions between air pollution and meteorological factors, as well as help refine meteorological and atmospheric chemistry models. In the future, we plan to combine field observation and numerical modeling for a more comprehensive, quantitative study of the interaction between aerosol, wind, and PBL under different weather regimes and geographic locations, in order to more fully characterize the nature of their interaction in the atmosphere.

Data availability. The meteorological data are provided by the data center of China Meteorological Administration (data link: http://data.cma.cn/en). The hourly pollutant data are released by the Ministry of Environmental Protection of China (data link: http://113.108.142.147:20035/emcpublish). The CALIPSO and MODIS data are obtained from the NASA Langley Research Center Atmospheric Science Data Center (data link: https://www.nasa.gov/langley). The MERRA reanalysis data are publicly available at https://disc.sci.gsfc.nasa.gov/datasets?page=1&keywords=merra. The AERONET data are publicly available at https://aeronet.gsfc.nasa.gov.

Competing interests. The authors declare that they have no conflict of interest.

Acknowledgements. This work is supported in part by grants from the National Science Foundation (NSF) (AGS1534670) and NSF of China (91544217) and NSF of US (). The authors would like to acknowledge the Department of Atmospheric and Oceanic Sciences of Peking University for providing the ground-based lidar data. We thank the Prof. Chengcai Li and Prof. Jing Li for theirs effort in establishing and maintaining the MPL site. We greatly appreciate the helpful advice from Prof. Jing Li and Prof. Chengcai Li at Peking University. We also thank the provision of surface pollutant data and meteorological data by the Ministry of Environmental Protection and China Meteorological Administration. We extend sincerest thanks to the CALIPSO, MODIS, AERONET, and MERRA teams for their datasets. The contributions of R. Kahn are supported in part by NASA's Climate and Radiation Research and Analysis Program under H. Maring, NASA's Atmospheric Composition Modeling and Analysis Program under R. Eckman.

Atmos. Chem. Phys. Discuss., https://doi.org/10.5194/acp-2018-279
Manuscript under review for journal Atmos. Chem. Phys.
Discussion started: 1 June 2018

Atmospheric Chemistry and Physics Discussions

References

Ackerman, A. S., Kirkpatrick, M. P., Stevens, D. E., and Toon, O. B.: The impact of humidity above stratiform clouds on indirect aerosol climate forcing. *Nature*, *432*, 1,014–1,017. https://doi.org/10.1038/nature03174, 2004

Boucher, O., Randall, D., Artaxo, P., Bretherton, C., Feingold, G., Forster, P., …, Zhang, X. Y.: Clouds and aerosols. In T. F. Stocker et al. (Eds.), *Climate Change 2013: The Physical Science Basis. Contribution of Working Group I to the Fifth Assessment Report of the Intergovernmental Panel on Climate Change*. (pp. 571–657). Cambridge Univ. Press, Cambridge, U. K. and New York, NY, USA, 2013.

Cai, Y. F., Wang, T. J., Xie, M., and Han, Y.: Impacts of atmospheric particles on surface ozone in Nanjing. *Climatic and Environmental Research*, *18*, 251–260, 2013.

Chan, C. K., and Yao, X.: Air pollution in megacities in China. *Atmospheric Environment*, *42*, 1–42. https://doi.org/10.1016/j.atmosenv.2007.09.003, 2008.

Cohn, S. A., and Angevine, W. M.: Boundary layer height and entrainment zone thickness measured by lidars and wind-profiling radars. *Journal of Applied Meteorology*, *39*, 1,233–1,247. https://doi.org/10.1175/1520-0450(2000)039<1233:BLHAEZ>2.0.CO;2, 2000.

Davis, K. J., Gamage, N., Hagelberg, C. R., Kiemle, C., Lenschow, D. H., and Sullivan P. P.: An objective method for deriving atmospheric structure from airborne lidar observations. *Journal of Atmospheric and Oceanic Technology*, *17*(11), 1,455–1,468. https://doi.org/10.1175/1520-0426(2000)017<1455:AOMFDA>2.0.CO;2, 2000.

Deng, X. J., Zhou, Tie, X. J., Wu, D., Li, F., … Deng, T.: Attenuation of ultraviolet radiation reaching the surface due to atmospheric aerosols in Guangzhou. *Science Bulletin*, *57*(21), 2,759–2,766. https://doi.org/10.1007/s11434-012-5172-5, 2012.

Ding, A., Huang, X., Nie, W., Sun, J. N., Kerminen, V.-M., Petäjä, T., … Fu, C. B.: Enhanced haze pollution by black carbon in megacities in China. *Geophysical Research Letters*, *43*, 2,873–2,879. https://doi.org/10.1002/2016GL067745, 2016.

Dong, Z., Li, Z., Yu, X., Cribb, M., Li, X., and Dai, J.: Opposite long-term trends in aerosols between low and high altitudes: a testimony to the aerosol–PBL feedback. *Atmospheric Chemistry and Physics*, *17*(12), 7,997–8,009. https://doi.org/10.5194/acp-17-7997-2017, 2017.

Emeis, S., and Schäfer, K.: Remote sensing methods to investigate boundary-layer structures relevant to air pollution in cities. *Boundary-layer meteorology*, 121(2), 377-385, 2006.

Flamant, C., Pelon, J., Flamant, P. H., and Durand, P.: Lidar determination of the entrainment zone thickness at the top of the unstable marine atmospheric boundary layer, *Boundary-Layer Meteorology*, *83*(2), 247–284. https://doi.org/10.1023/A:1000258318944, 1997.

Guo, J., Miao, Y., Zhang, Y., Liu, H., Li, Z., Zhang, W., … and Zhai, P: The climatology of planetary boundary layer height in China derived from radiosonde and reanalysis data. *Atmospheric Chemistry and Physics*, *16*(20), 13,309–13,319. https://doi.org/10.5194/acp-16-13309-2016, 2016.

Guo, J., Su, T., Li, Z., Miao, Y., Li, J., Liu, H., … Zhai, P.: Declining frequency of summertime local-scale precipitation over eastern China from 1970 to 2010 and its potential link to aerosols. *Geophysical Research Letters*, *44*(11), 5,700–5,708. https://doi.org/10.1002/2017GL073533, 2017.

Guo, S., Hu, M., Zamora, M. L., Peng, J., Shang, D., Zheng, J., … Zhang, R.: Elucidating severe urban haze formation in China. *Proceedings of the National Academy of Science USA*, *111*, 17,373–17,378. https://doi.org/10.1073/pnas.1419604111, 2014.

Hägeli, P., Steyn, D., and Strawbridge, K.: Spatial and temporal variability of mixed-layer depth and entrainment zone thickness. *Boundary-Layer Meteorology*, *97*(1), 47–71. https://doi.org/10.1023/A:1002790424133, 2000.

He, Q., Li, C., Mao, J., Lau, A. K.-H., and Chu, D. A.: Analysis of aerosol vertical distribution and variability in Hong Kong. *Journal of Geophysical Research: Atmospheres*, *113*, D14211. https://doi.org/10.1029/2008JD009778, 2008.

Hooper, W. P., and Eloranta, E. W.: Lidar measurements of wind in the planetary boundary layer – the method, accuracy and results from joint measurements with radiosonde and kytoon. *Boundary-Layer Meteorology*, *25*(7), 1986.

Huang, R. J., Zhang, Y., Bozzetti, C., Ho, K. F., Cao, J. J., Han, Y., ... and Zotter, P.: High secondary aerosol contribution to particulate pollution during haze events in China. Nature, 514(7521), 218. Jacob, DJ. Heterogeneous chemistry and tropospheric ozone. Atmos Environ 2000; 34(12): 2131-2159, 2014.

Johnson, R. H., Ciesielski, P. E., and Cotturone, J. A.: Multiscale variability of the atmospheric mixed layer over the western Pacific warm pool. *Journal of the Atmospheric Sciences*, *58*, 2,729–2,750, 2001.

Jordan, N. S., R. M. Hoff, and J. T. Bacmeister.: Validation of Goddard Earth Observing System-version 5 MERRA planetary boundary layer heights using CALIPSO, J. Geophys. Res., 115, D24218, doi:10.1029/2009JD013777, 2010.

Kiehl, J. T., and Briegleb, B. P.: The relative roles of sulfate aerosols and greenhouse gases in climate forcing. *Science*, *260*, 311–314. https://doi.org/10.1126/science.260.5106.311, 1993.

Knote, C., Tuccella, P., Curci, G., Emmons, L., Orlando, J. J., Madronich, S., … Zhang, Y.: Influence of the choice of gas-phase mechanism on predictions of key gaseous pollutants during the AQMEII phase-2 intercomparison. *Atmospheric Environment*, *115*, 553–568. https://doi.org/10.1016/j.atmosenv.2014.11.066, 2015.

L'Ecuyer, T. S., and Jiang, J. H.: Touring the atmosphere aboard the A-Train. *Physics Today*, *63*(7), 36–41, 2010.

LeMone, M. A., Tewari, M., Chen, F., and Dudhia, J.: Objectively determined fair-weather CBL depths in the ARW-WRF model and their comparison to CASES-97 observations. *Monthly Weather Review*, *141*, 30–54. https://doi.org/10.1175/MWR-D-12- 00106.1, 2013

Leventidou, E., Zanis, P., Balis, D., Giannakaki, E., Pytharoulis, I., and Amiridis, V.: Factors affecting the comparisons of planetary boundary layer height retrievals from CALIPSO, ECMWF and radiosondes over Thessaloniki, Greece. *Atmospheric Environment*, *74*, 360–366. https://doi.org/10.1016/j.atmosenv.2013.04.007, 2013.

Levy, R.C., Remer, L.A., Kleidman, R.G., Mattoo, S., Ichoku, C., Kahn, R., Eck, T.F.: Global evaluation of the Collection 5 MODIS dark-target aerosol products over land. Atmos. Chem. Phys. 10 (21), 10399e10420, 2010.

Li, J., Li, C., Zhao, C. and Su, T.: Changes in surface aerosol extinction trends over China during 1980 - 2013 inferred from quality - controlled visibility data. Geophysical Research Letters, 43(16), pp.8713-8719, 2016.

Li, J., Wang, Z., Wang, X., Yamaji, K., Takigawa, M., Kanaya, Y., … Akimoto, H.: Impacts of aerosols on summertime tropospheric photolysis frequencies and photochemistry over Central Eastern China. *Atmospheric Environment*, *45*(10), 1,817–1,829. https://doi.org/10.1016/j.atmosenv.2011.01.016, 2011.

Li, Z., Guo, J., Ding, A., Liao, H., Liu, J., Sun, Y., and Zhu, B. (2017). Aerosol and boundary-layer interactions and impact on air quality. *National Science Review*, nwx117. https://doi.org/10.1093/nsr/nwx117, 2017.

Li, Z., Lau, W. K.-M., Ramanathan, V., Wu, G., Ding, Y., Manoj, M. G., … Brasseur, G. P.: Aerosol and monsoon climate interactions over Asia. *Reviews of Geophysics*, *54*, 866–929. https://doi.org/10.1002/2015RG000500, 2016.

Li, Z., Rosenfeld, D., Fan, J.: Aerosols and their Impact on Radiation, Clouds, Precipitation and Severe Weather Events, Oxford Encyclopedia in Environmental Sciences, 10.1093/acrefore/9780199389414.013.126, 2017a,

Liao, H., and Seinfeld, J. H.: Global impacts of gas - phase chemistry - aerosol interactions on direct radiative forcing by anthropogenic aerosols and ozone. Journal of Geophysical Research: Atmospheres, 110(D18), 2005.

Liu, J., Huang, J., Chen, B., Zhou, T., Yan, H., Jin, H., … Zhang, B.: Comparisons of PBL heights derived from CALIPSO and ECMWF reanalysis data over China. *Journal of Quantitative Spectroscopy and Radiative Transfer*, *153*, 102–112. https://doi.org/10.1016/j.jqsrt.2014.10.011, 2015.

Liu, S., and Liang, X.-Z.: Observed diurnal cycle climatology of planetary boundary layer height. *Journal of Climate*, *22*(21), 5,790–5,809. https://doi.org/10.1175/ 2010JCLI3552.1, 2010.

McGrath-Spangler, E. L., and Denning, A. S.: Estimates of North American summertime planetary boundary layer depths derived from space-borne lidars. *Journal of Geophysical Research: Atmospheres*, *117*. https://doi.org/10.1029/012JD017615, 2012.

Melfi, S. H., Whiteman, D., and Ferrare, R.: Observation of atmospheric fronts using Raman lidar moisture measurements. *Journal of Applied Meteorology*, *28*(9), 789–806. https://doi.org/10.1175/1520-0450(1989)028<0789:OOAFUR>2.0.CO;2, 1989.

Miao, Y., Guo, J., Liu, S., Liu, H., Li, Z., … Zhai, P.: Classification of summertime synoptic patterns in Beijing and their associations with boundary layer structure affecting aerosol pollution. *Atmospheric Chemistry and Physics*, *17*, 3,097–3,110. https://doi.org/10.5194/acp-17-3097-2017, 2017.

Miao, Y., Liu, S., Zheng, Y., and Wang, S.: Modeling the feedback between aerosol and boundary layer processes: a case study in Beijing, China. *Environmental Science and Pollution Research*, *23*(4), 3,342–3,357. https://doi.org/10.1007/s11356-015-5562-8, 2016.

Mok, M., et al.: Impacts of brown carbon from biomass burning on surface UV and ozone photochemistry in the Amazon Basin, *Scientific Report,* DOI: 10.1038/srep36940, 2016.

Petäjä, T., Järvi, L., Kerminen, V.-M., Ding, A. J., Sun, J. N., Nie, W., … Kulmala, M.: Enhanced air pollution via aerosol-boundary layer feedback in China. *Scientific Reports*, *6*. https://doi.org/10.1038/srep18998, 2016.

Qu, Y., Han, Y., Wu, Y., Gao, P. and Wang, T.: Study of PBLH and Its Correlation with Particulate Matter from One-Year Observation over Nanjing, Southeast China. Remote Sensing, 9(7), p.668, 2017.

Ravishankara, AR. Heterogeneous and multiphase chemistry in the troposphere. Science, 276(5315): 1058-1065, 1997.

Sawyer, V., and Li, Z.: Detection, variations and intercomparison of the planetary boundary layer depth from radiosonde, lidar and infrared spectrometer. *Atmospheric Environment*, *79*, 518–528. https://doi.org/10.1016/j.atmosenv.2013.07.019, 2013.

Schafer, J. S., Eck, T. F., Holben, B. N., Thornhill, K. L., Anderson, B. E., Sinyuk, A., ... and Kenny, P. R.: Intercomparison of aerosol single - scattering albedo derived from AERONET surface radiometers and LARGE in situ aircraft profiles during the 2011 DRAGON - MD and

Atmos. Chem. Phys. Discuss., https://doi.org/10.5194/acp-2018-279
Manuscript under review for journal Atmos. Chem. Phys.
Discussion started: 1 June 2018

DISCOVER‐AQ experiments. *Journal of Geophysical Research: Atmospheres*, 119(12), 7439-7452, 2014.

Seibert, P., Beyrich, F., Gryning, S.-E., Joffre, S., Rasmussen, A., and Tercier, P.: Review and intercomparison of operational methods for the determination of the mixing height. *Atmospheric Environment*, *34*(7), 1,001–1,027. https://doi.org/10.1016/S1352-2310(99)00349-0, 2000.

Su, T., Li, J., Li, C., Lau, A. K. H., Yang, D., and Shen, C.: An intercomparison of AOD-converted PM2.5 concentrations using different approaches for estimating aerosol vertical distribution. *Atmospheric Environment*, 166, 531-542, 2017a.

Su, T., Li, J., Li, C., Xiang, P., Lau, A.K.H., Guo, J., Yang, D. and Miao, Y.: An intercomparison of long‐term planetary boundary layer heights retrieved from CALIPSO, ground‐based lidar, and radiosonde measurements over Hong Kong. Journal of Geophysical Research: Atmospheres, 122(7), pp.3929-3943, 2017b.

Tang, G., Zhang, J., Zhu, X., Song, T., Münkel, C., Hu, B., … Wang, Y.: Mixing layer height and its implications for air pollution over Beijing, China. *Atmospheric Chemistry and Physics*, *16*, 2,459–2,475. https://doi.org/10.5194/acp-16-2459-2016, 2016.

Tie, X., Zhang, Q., He, H., Cao, J., Han, S., Gao, Y., Li, X. and Jia, X.C.: A budget analysis of the formation of haze in Beijing. Atmospheric Environment, 100, pp.25-36, 2015.

Tucker, S. C., Senff, C. J., Weickmann, A. M., Brewer, W. A., Banta, R. M., Sandberg, S. P., … Hardesty, R. M.: Doppler lidar estimation of mixing height using turbulence, shear, and aerosol profiles. *Journal of Atmospheric and Oceanic Technology*, *26*(4), 673–688. https://doi.org/10.1175/2008JTECHA1157.1, 2009.

Vogelezang, D. H. P., and Holtslag, A. A. M.: Evaluation and model impacts of alternative boundary layer height formulations. *Boundary-Layer Meteorology*, *81*(3-4), 245–269. https://doi.org/10.1007/BF02430331, 1996.

Wang, G., Zhang, R., Gomez, M. E., Yang, L., Zamora, M. L., Hu, M., … Molina, M. J.: Persistent sulfate formation from London fog to Chinese haze. *Proceedings of the National Academy of Science USA*, *113*, 13,630–13,635. https://doi.org/10.1073/pnas.1616540113, 2016.

Wang, X., Dickinson, R. E., Su, L., Zhou, C., and Wang, K.: PM2.5 pollution in China and how it has been exacerbated by terrain and meteorological conditions. Bulletin of the American Meteorological Society. https://doi.org/10.1175/BAMS-D-16-0301.1, 2017.

Wang, Y., Khalizov, A., and Zhang, R.: New directions: light-absorbing aerosols and their atmospheric impacts. *Atmospheric Environment*, *81*, 713–715. https://doi.org/10.1016/j.atmosenv.2013.09.034, 2013.

Winker, D. M., Hunt, W. H., and McGill, M. J.: Initial performance assessment of CALIOP. *Geophysical Research Letters*, *34*, L19803. https://doi.org/10.1029/ 2007GL030135, 2007.

Winker, D. M., Vaughan, M. A., Omar, A., Hu, Y., Powell, K. A., Liu, Z., … Young, S. A.: Overview of the CALIPSO mission and CALIOP data processing algorithms. *Journal of Atmospheric and Oceanic Technology*, *26*, 2,310–2,323. https://doi.org/10.1175/2009JTECHA1281.1, 2009.

Yang, D., Li, C., Lau, A. K. H., and Li, Y.: Long-term measurement of daytime atmospheric mixing layer height over Hong Kong. *Journal of Geophysical Research: Atmospheres*, *118*, 2,422–2,433. https://doi.org/10.1002/jgrd.50251, 2013.

Zhang, W., Guo, J., Miao, Y., Liu, H., Zhang, Y., Li, Z., and Zhai, P.: Planetary boundary layer height from CALIOP compared to radiosonde over China. *Atmospheric Chemistry and Physics*, *16*, 9,951–9,963. https://doi.org/10.5194/acp-16-9951-2016., 2016.

Table 1.

Mean values and standard deviation (STD) of CALIPSO-PBLH, MERRA-PBLH, and $PM_{2.5}$ over different ROIs.

Parameter			NCP	PRD	YRD	NEC
CALIPSO-PBLH (km)	MAM	Mean	1.40	1.35	1.31	1.40
		STD	0.54	0.47	0.48	0.59
	JJA	Mean	1.47	1.27	1.24	1.46
		STD	0.51	0.44	0.46	0.55
	SON	Mean	1.21	1.24	1.26	1.15
		STD	0.45	0.36	0.39	0.50
	DJF	Mean	1.06	1.07	1.12	0.94
		STD	0.40	0.34	0.41	0.47
MERRA-PBLH (km)	MAM	Mean	1.57	1.16	1.24	1.45
		STD	0.75	0.53	0.47	0.69
	JJA	Mean	1.46	0.99	1.07	1.49
		STD	0.72	0.36	0.39	0.68
	SON	Mean	1.37	1.18	1.22	1.19
		STD	0.48	0.37	0.33	0.54
	DJF	Mean	1.08	1.09	1.05	0.65
		STD	0.36	0.40	0.32	0.36
$PM_{2.5}$ ($\mu g\ m^{-3}$)	MAM	Mean	63.1	32.8	50.4	34.8
		STD	45.1	22.1	29.2	29.4
	JJA	Mean	51.2	25.1	37.9	29.6
		STD	36.8	20.4	24.1	24.4
	SON	Mean	70.9	39.3	42.4	44.2
		STD	58.4	23.1	28.3	49.1
	DJF	Mean	102.7	44.2	69.8	60.3
		STD	84.2	28.3	51.3	54.4

Atmos. Chem. Phys. Discuss., https://doi.org/10.5194/acp-2018-279
Manuscript under review for journal Atmos. Chem. Phys.
Discussion started: 1 June 2018

Atmospheric Chemistry and Physics
Discussions

671

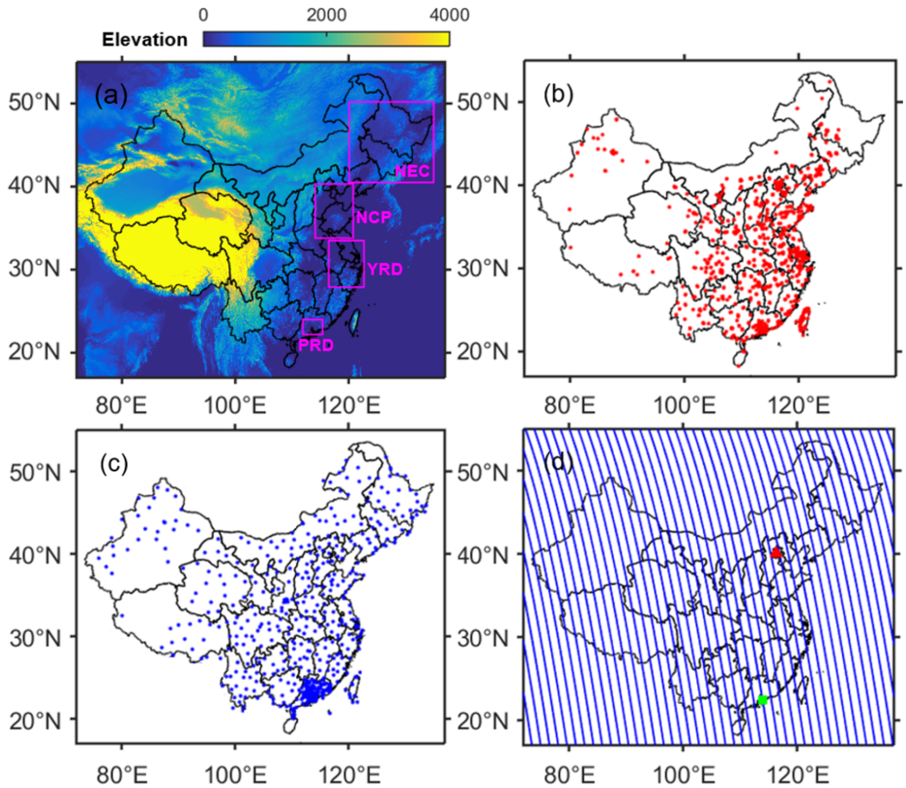

672 **Figure 1.** (a) Topography of China. The black rectangles outline the five regions of interest: northeast
673 China (NEC): 40.5-50.2°N, 120.1-135°E; North China Plain (NCP): 33.8-40.3°N, 114.1-120.8°E; Pearl
674 River Delta (PRD): 22.2-24°N, 111.9-115.4°E; and Yangtze River Delta (YRD): 27.9-33.5°N, 116.5-
675 122.7°E. Locations of (b) environmental stations and (c) meteorological stations. (d) Blue lines indicate
676 CALIOP daytime orbits (in ascending node). Ground-based lidar and sun-photometer are deployed at
677 Beijing (red circle), and sun-photometer is deployed at Hong Kong (green circle).

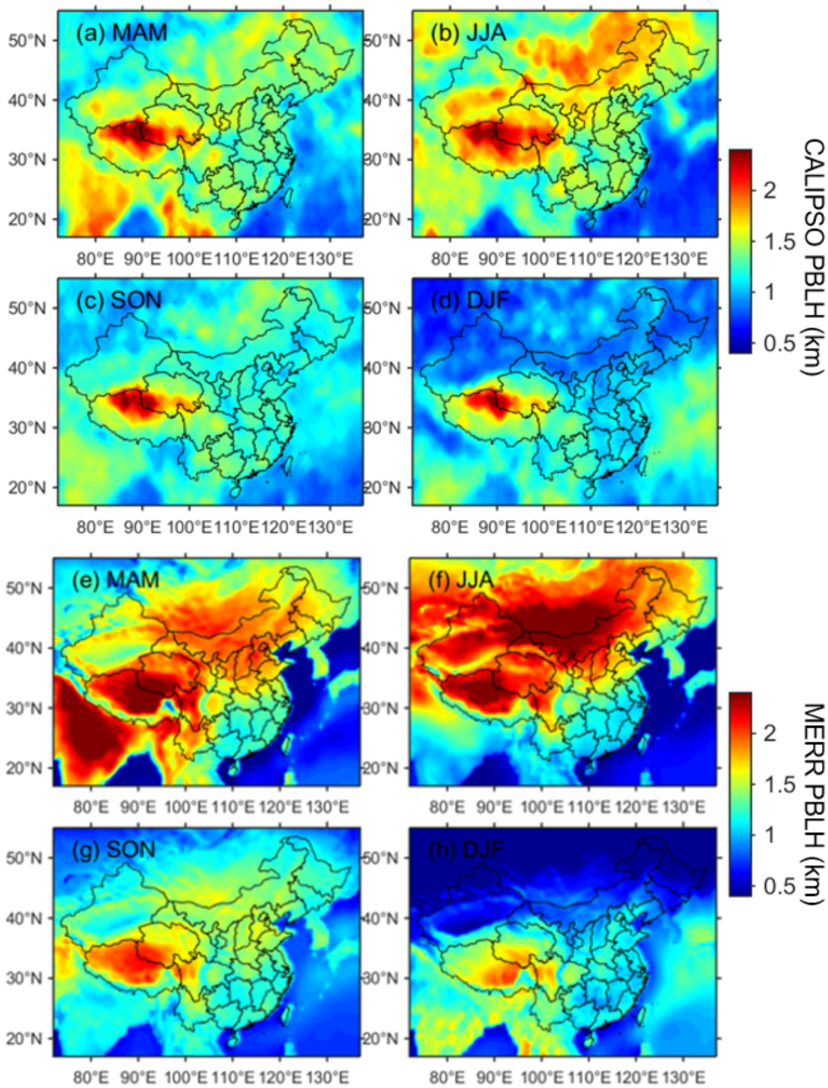

Figure 2. Spatial distributions of climatological mean PBLH derived from CALIPSO for (a) March-April-May (MAM), (b) June-July-August (JJA), (c) September-October-November (SON), and (d) December-January-February (DJF) during the period 2006–2017. Spatial distributions of climatological mean noontime PBLH obtained from MERRA for (e) MAM, (f) JJA, (g) SON, and (h) DJF during the same period.

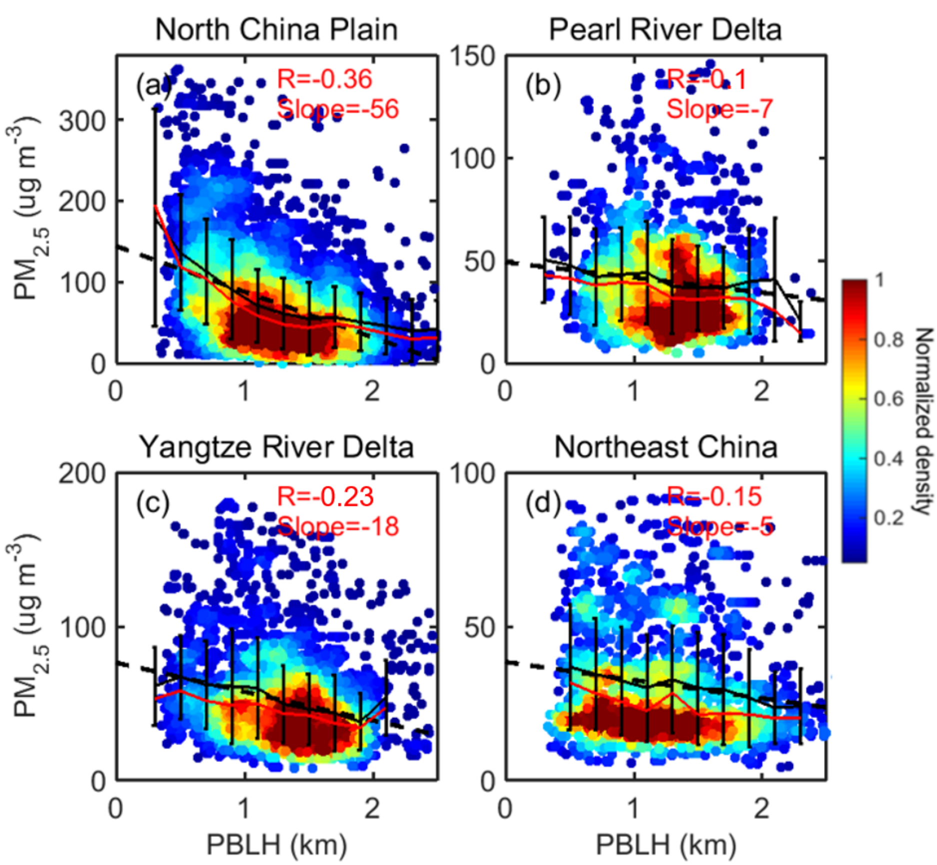

Figure 3. The relationship between CALIPSO-derived PBLH and noontime $PM_{2.5}$ over (a) NCP, (b) PRD, (c) YRD, and (d) NEC. The black solid lines represent the average values for each bin, and whiskers indicate one standard deviation. The red solid lines highlight the median for each bin, and the black dashed lines give the linear regressions. The correlation coefficients and slopes for these relationships are shown at the top of each panel. The color-shaded dots indicate the normalized sample density.

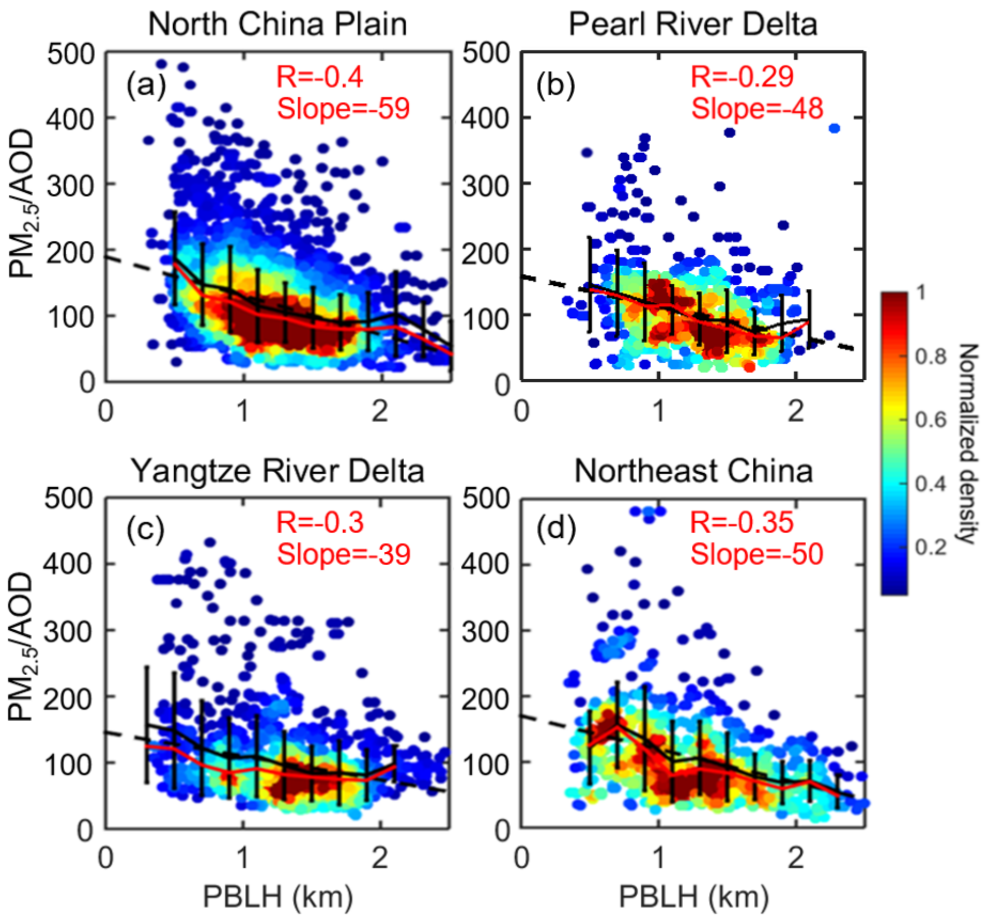

Figure 4. Similar to Figure 3, but for the relationship between CALIPSO PBLH and noontime $PM_{2.5}$/AOD (unit: μg m^{-3} per AOD) over four ROIs.

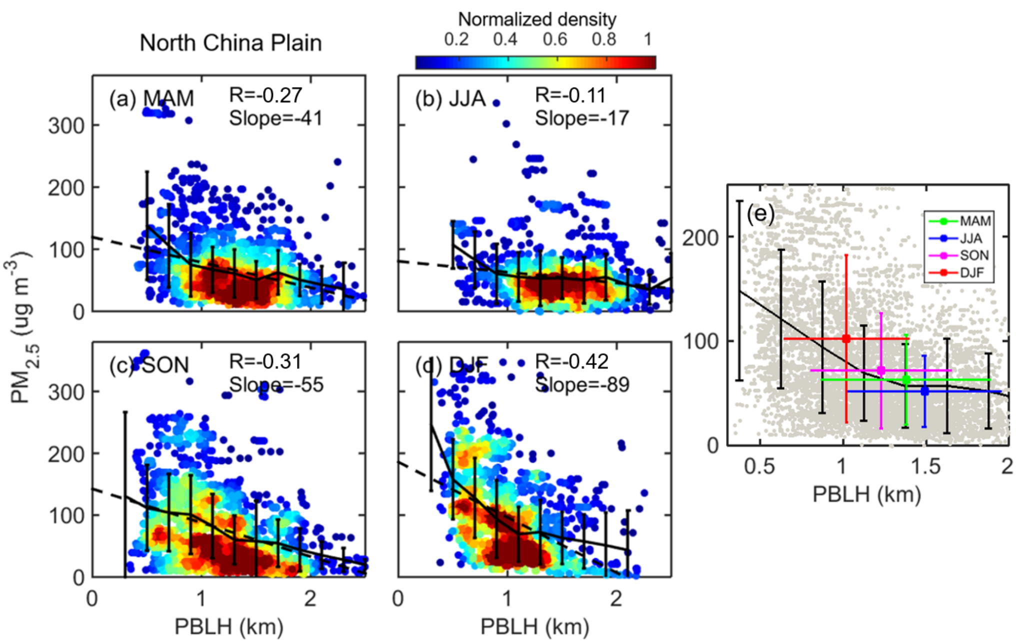

Figure 5. The relationship between CALIPSO PBLH and $PM_{2.5}$ over the NCP for (a) MAM, (b) JJA, (c) SON, and (d) DJF. (e) General relationship between $PM_{2.5}$ and PBLH aggregated over all seasons, with individual observations for each day plotted as gray dots. The green, blue, pink, and red dots present the mean values for MAM, JJA, SON, and DJF, respectively.

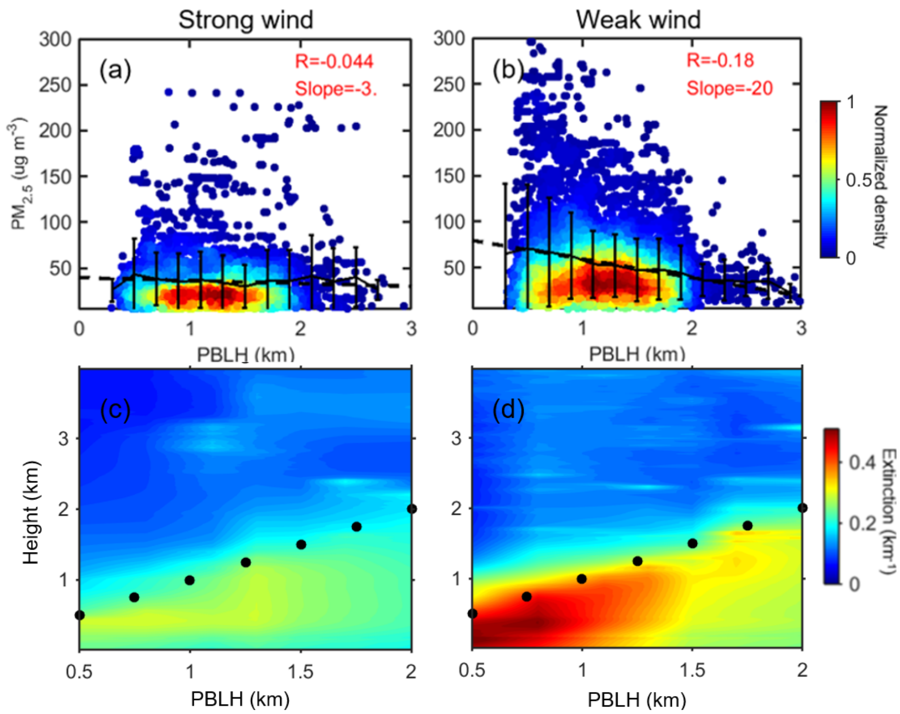

Figure 6. The relationship between CALIPSO PBLH and $PM_{2.5}$ over China for (a) strong wind (WS>4m s^{-1}) and (b) weak wind (WS<4m s^{-1}). The aerosol extinction profiles at ~550 nm derived from MPL at Beijing change with different MPL-derived PBLH under (c) strong wind and (d) weak wind conditions. In (c, d), the black dots indicate the location of PBL top.

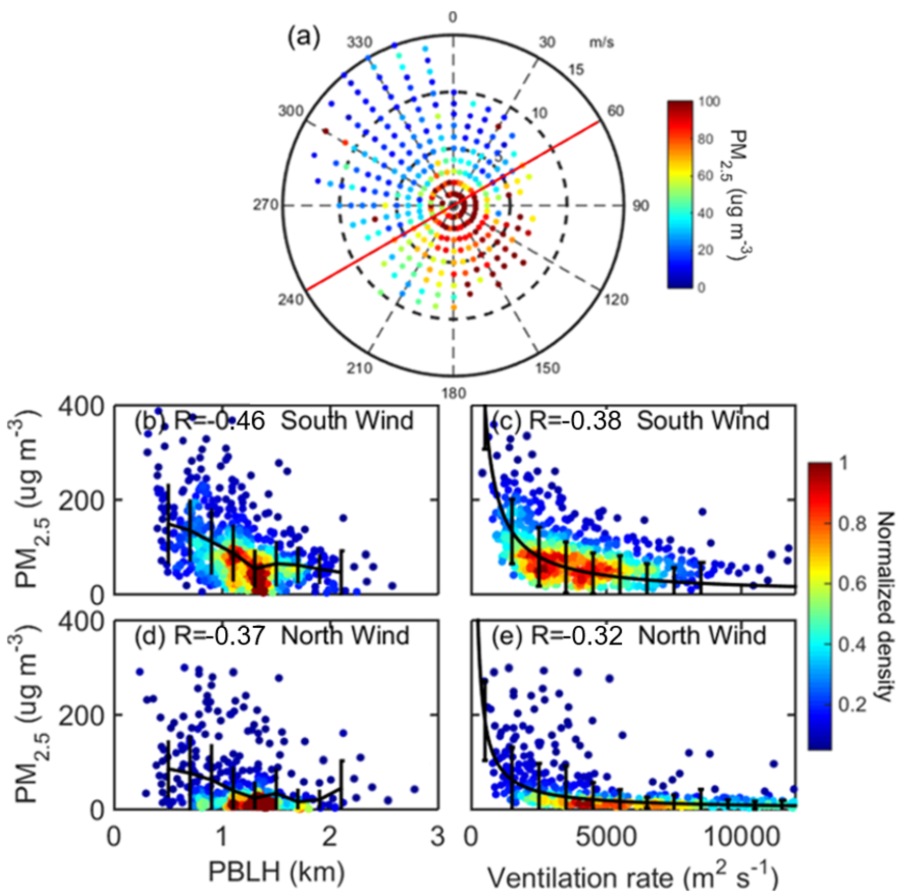

Figure 7. (a) Relationship between wind direction/wind speed and $PM_{2.5}$ over Beijing. The red line divides the northerly wind and southerly wind. (b-c) The relationship between $PM_{2.5}$ and MPL-PBLH/ventilation rate (VR = WS × PBLH), for southerly winds over Beijing. (d-e) The relationship between $PM_{2.5}$ and MPL-PBLH/VR, for northerly winds over Beijing.

Atmos. Chem. Phys. Discuss., https://doi.org/10.5194/acp-2018-279
Manuscript under review for journal Atmos. Chem. Phys.
Discussion started: 1 June 2018

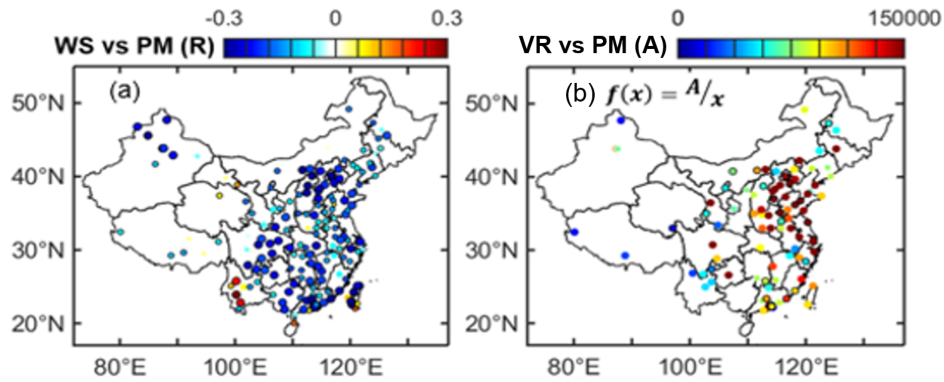

Figure 8. (a) Spatial distribution of correlation coefficients (R) for the WS-$PM_{2.5}$ relationship. (b) Spatial distribution of fitting parameter (A) for the VR-$PM_{2.5}$ relationship. The function $f(x) = A/x$ is used to characterize the relationship between VR and $PM_{2.5}$, with A as the fitting parameter, and x is VR, and $f(x)$ is $PM_{2.5}$. Both WS and $PM_{2.5}$ are obtained from surface data, and PBLH are derived from CALIPSO. Dots marked with black circles indicate where the relationship is statistically significant at the 95% confidence level.

Atmos. Chem. Phys. Discuss., https://doi.org/10.5194/acp-2018-279
Manuscript under review for journal Atmos. Chem. Phys.
Discussion started: 1 June 2018

Atmospheric Chemistry and Physics
Discussions

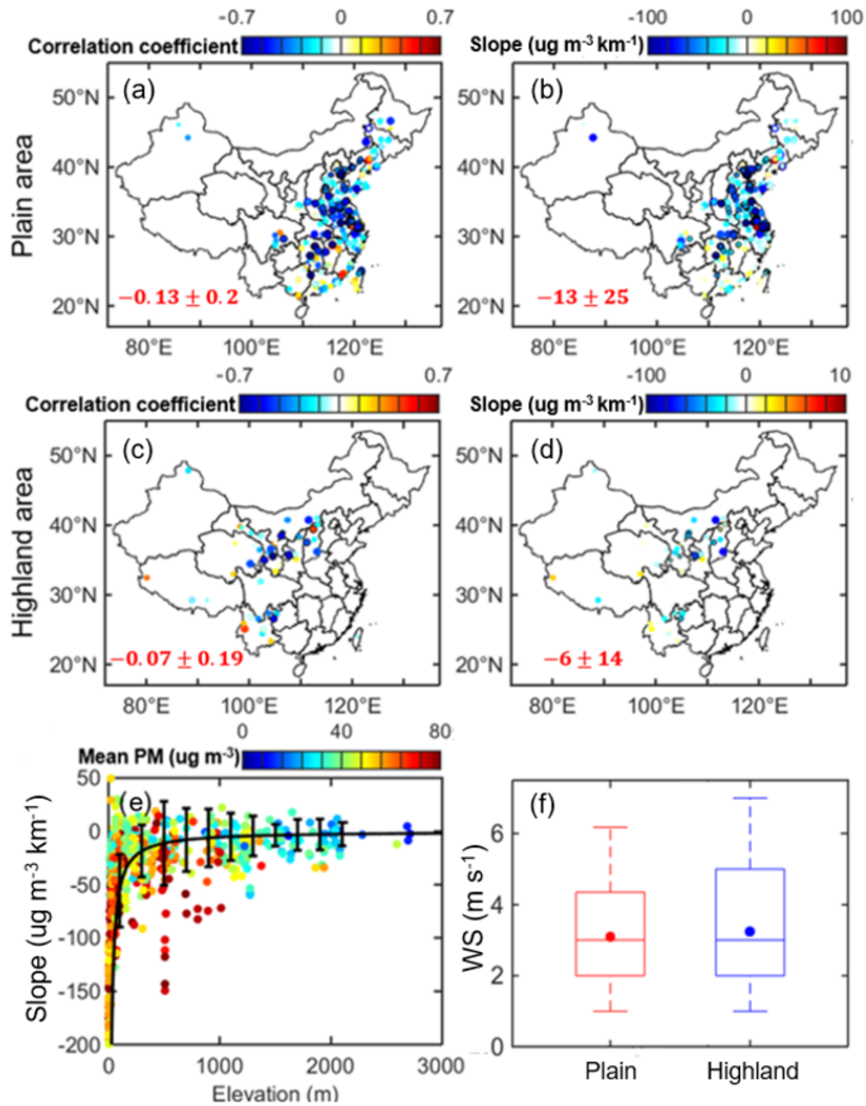

Figure 9. Stratification by terrain elevation. The correlation coefficients (R) and slopes between CALIPSO PBLH and noontime $PM_{2.5}$ for plain areas (a-b) and highland areas (c-d). (e) The relationship between PBLH- $PM_{2.5}$ slope and station elevation, with color-shading indicating station mean $PM_{2.5}$ concentration. (f) Box-and-whisker plots showing the 10th, 25th, 50th, 75th, and 90th percentile values of the noontime WS for plain and highland regions. The dots indicate the mean value.

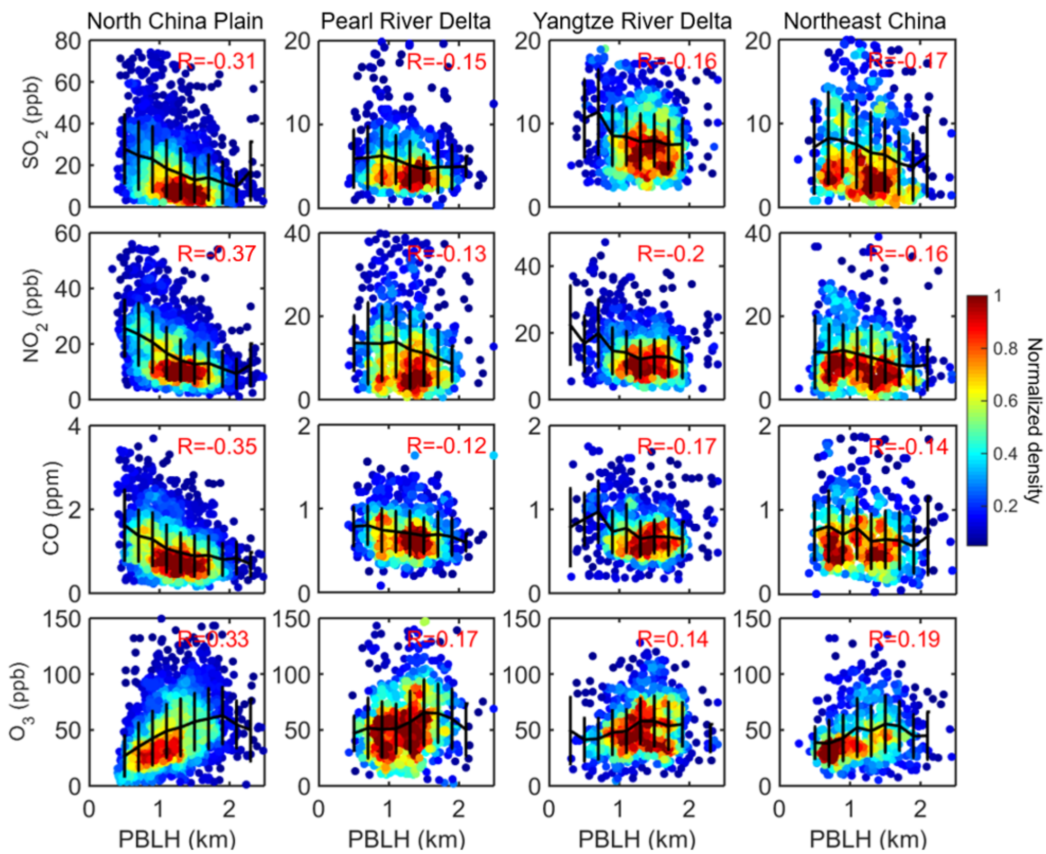

Figure 10. The relationships between CALIPSO-derived PBLH and multiple gas pollutants over (from left to right) the NCP, PRD, YRD, and NEC. The color-shaded dots indicate the normalized sample density. Correlation coefficients (R) are shown in red in each panel.

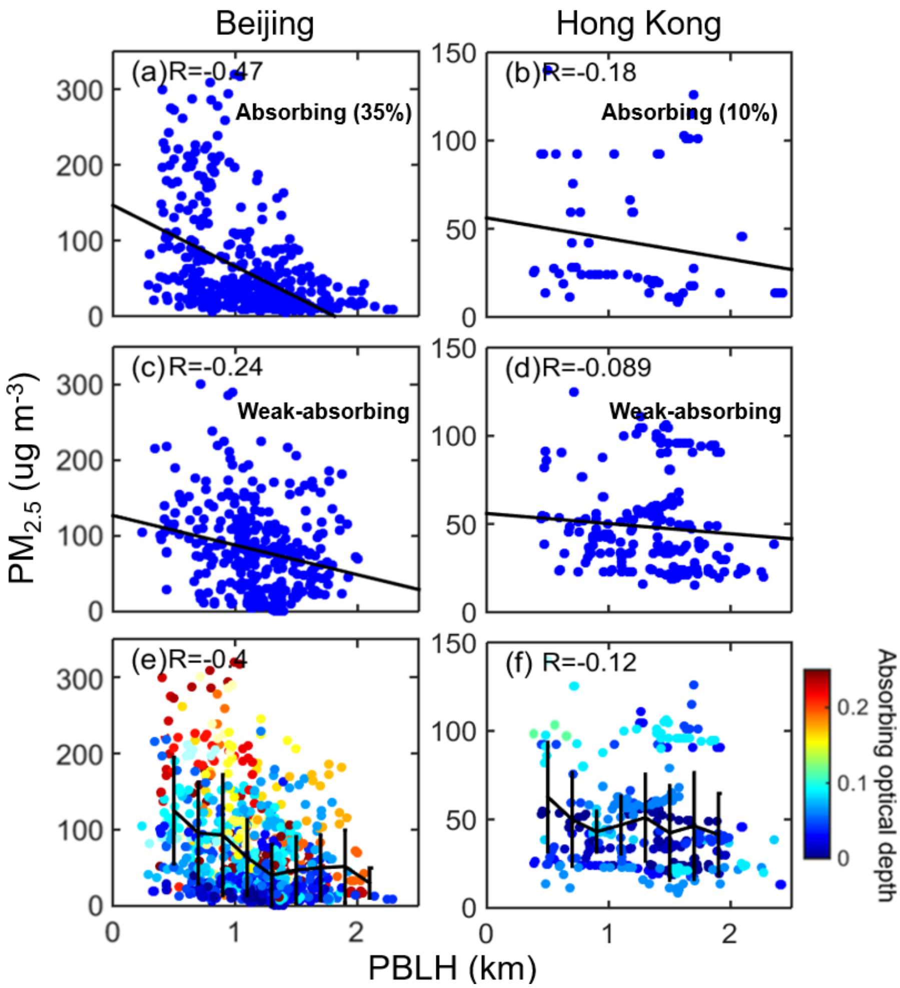

Figure 11. The relationship between $PM_{2.5}$ and PBLH for absorbing aerosols over (a) Beijing and (b) Hong Kong. The percentage of absorbing cases are noted in (a) and (b). The relationship between $PM_{2.5}$ and PBLH for weakly absorbing aerosols over (c) Beijing and (d) Hong Kong. In (a, b, c, d), color bars represent normalized density. The relationship between total $PM_{2.5}$ and PBLH over (e) Beijing and (f) Hong Kong. In (e, f), the color-shaded dots indicate absorbing optical depth. The PBLHs over Beijing are obtained from MPL, and the PBLHs over Hong Kong are calculated by CALIPSO.